Supporting Information

Quantification of Plasma-Produced Hydroxyl Radicals in Solution and their Dependence on the pH

Francesco Tampieri[a,b,c], Maria-Pau Ginebra[a,b,c,d] and Cristina Canal[a,b,c]

[a] Biomaterials, Biomechanics and Tissue Engineering Group, Department of Materials Science and Metallurgy, Universitat Politècnica de Catalunya, c. Eduard Maristany 16, 08019 Barcelona, Spain.

[b] Barcelona Research Center in Multiscale Science and Engineering, Universitat Politècnica de Catalunya, Barcelona, Spain.

[c] Research Centre for Biomedical Engineering, Universitat Politècnica de Catalunya, Barcelona, Spain.

[d] Institute for Bioengineering of Catalonia, Barcelona Institute of Science and Technology, Barcelona, Spain

Experimental section

Materials. Terephthalic acid disodium salt (TPA, $C_8H_4O_4Na_2$, >99%) was purchased from Alfa Aesar. 2-hydroxyterephthalic acid (hTPA, $C_8H_6O_5$, 97%) was purchased from Sigma Aldrich. Phosphoric acid (H_3PO_4, 85.0-88.0%) and disodium hydrogen phosphate dodecahydrate ($Na_2HPO_4 \cdot 12H_2O$, >98.0%) were purchased from Panreac. Sodium dihydrogen phosphate dihydrate ($NaH_2PO_4 \cdot 2H_2O$, >98.0%) was purchased by Merck. Acetonitrile (ACN, 99.9%) was purchased by Carlo Erba Reagents. Ultrapure water was obtained by filtration using 0.22-µm pore size MILLEXGP filter unit (Merck Millipore Ltd., Ireland). Helium gas (99.998%, maximum impurities of O_2 and H_2O 5 ppm_v) was provided by Praxair, Spain.

Plasma source and treatments. The plasma source used in this work is an atmospheric pressure plasma jet (APPJ) that was already described in detail in previous publications.[1,2] The active electrode is a copper wire (0.1 mm diameter) embedded inside a quartz tube (ID = 1.2 mm) and connected to a high voltage power supply. The discharge was operated with a sinusoidal waveform at 23 kHz with (U) ~ 2 kV and (I) ~ 3 mA. The average power delivered to the discharge was 1 W. Pure He flows through the tube and serves as plasma feed gas. A Bronkhorst MASS-VIEW flow controller was used to set the gas flow rate. Experiments were performed in open air, at room temperature and with an average relative humidity of 70%.

All the treatments, if not otherwise stated, were done using the following conditions: He flow rate 1 L min^{-1}, distance between plasma nozzle and target 10 mm, sample volume 1 mL, sample support 24 well plate (Thermo Scientific, Nunclon Delta Surface), according to previous works.[3] Treatment time was generally varied between 30 to 300 s. The He flow was started 15-20 min before each treatment in order to ensure a good purge of the gas line (checked by optical emission spectroscopy). The plasma was started at least 5-10 min before the treatment to let it stabilize. Each plasma treatment was repeated four times to ensure reproducibility.

Experimental procedures. All solutions used for plasma treatments were prepared in 100 mM phosphate buffer (PB) at pH 7, typical of physiological conditions, or pH 3, which is a value typically reached by a 5-10 min APPJ treatment of non-buffered water solutions.[4] Stocks of buffer solutions were prepared by dissolving the required amount of phosphate salts ($Na_2HPO_4 \cdot 12H_2O$ and $NaH_2PO_4 \cdot 2H_2O$) or phosphoric acid in ultrapure water and adjusting the final pH, if necessary, with small volumes of 1 M solutions of HNO_3 or NaOH. We avoided chloride ions in our experiments (PBS or HCl for pH adjustment) because they are known to react with HO radicals generated by plasma and would possibly affect the reactivity of the system.[5]

10^{-2} M and 10^{-4} M TPA stock solutions were prepared by directly dissolving the powder in buffer, respectively at pH 7 and 3. Different concentrations of TPA were used because at pH 3 terephthalate is protonated (terephthalic acid, pK_a = 3.51, 4.82[6]) and thus much less soluble (solubility 10^{-4} M ca.[7]). The concentration ranges were 15-100 μM at pH 3 and 50-5000 μM at pH 7.

After plasma treatment, 0.5 mL of each treated solutions were transferred to a 48 well plate for fluorescence measurements and 100 μL were diluted 1:10 with PB 20 mM pH 1.5 inside 2 mL HPLC vials and analysed by HPLC/UV-Vis. This dilution serves to bring the residual TPA concentration in the right range for the analysis and ensures that during the analysis both the carboxylic groups are protonated, regardless of the pH of the initial buffer.

Fluorescence measurements were performed using a Synergy HTX Hybrid Multi Mode Microplate Reader (BioTek Instruments, Inc., USA), with fluorescence filters centred at λ_{ex} = 360/40 nm and λ_{em} = 460/40 nm as excitation and emission wavelengths, respectively. Calibration lines for fluorescence were made measuring the fluorescence signal of standard solutions of hTPA in PB at pH 3 and 7 under the same conditions.

HPLC/UV-Vis measurements were done using a Shimadzu Prominence XR instrument with autosampler and UV/VIS photodiode array detector equipped with a Waters xBridge BEH130C18 analytical column (3.5 um 4.6x100 mm). Eluents were PB 20 mM pH 1.5 (A) and acetonitrile (B). Elution was isocratic (A:B 85:15), flow rate was 1 mL min^{-1} and detection 190-400 nm. Under these conditions, retention time for TPA was 3.2 min and for hTPA 4.1 min. Calibration lines were obtained analysing, under the same conditions, standard solutions of TPA and hTPA in PB 20 mM pH 1.5.

Since small volumes were treated, water evaporation during the plasma treatment affects the concentrations measured, particularly for the longest treatment times. Therefore, the evaporation rate was measured under the conditions used during the experiments ($(2.10 \pm 0.09)\cdot 10^{-4}$ s^{-1}) and was used to correct the fluorescence intensities and HPLC areas accordingly.

Data elaboration. To determine quantitative parameters about OH radicals generated by cold plasma we adapted the procedure described by Anifowose et al. for the quantification of superoxide in seawaters[8] and recently used for quantification of plasma-generated superoxide in water solutions.[9]

If we consider the general reaction between a short-lived reactive species (*RS*) with a chemical probe (*Probe*) in solution that traps it and forms a stable product (*Product*) that can therefore be detected analytically

$$RS + Probe \xrightarrow{k_{Probe}} Product \qquad \text{(S1)}$$

where k_{Probe} is the kinetic constant of the reaction. A necessary requisite is that *Product* is generated only by reaction of *Probe* with *RS* and not with other species in the system. In our case *RS* is HO radical, *Probe* is TPA and *Product* is hTPA.

The formation rate of *RS* in solution (R_{RS}), its lifetime ($t_{1/2}$) and its steady-state concentration ($[RS]_{SS}$) can be defined as

$$R_{RS} = \frac{R_{Product}}{Y_{Product} \cdot F_{RS}} \tag{S2}$$

$$t_{1/2} = \frac{\ln(2)}{\sum k_S[S]} \tag{S3}$$

$$[RS]_{SS} = \frac{R_{RS}}{k_{Probe}[Probe]_0 + \sum k_S[S]} \tag{S4}$$

where $R_{Product}$ is the formation rate of *Product* in solution and can be determined experimentally; $Y_{Product}$ is the yield of *Product* formed per reaction of *Probe* with *RS*; F_{RS} is the fraction of *RS* that reacts with *Probe*, $\sum k_S[S]$ is a term that takes into account all the other processes, *S* being all other scavengers that can react with *RS*, other than *Probe*, and that lead to *RS* consumption and $[Probe]_0$ is *Probe* initial concentration. $Y_{Product}$ and F_{RS} are defined as

$$Y_{Product} = \frac{R_{Product}}{R_{Probe}} \tag{S5}$$

$$F_{RS} = \frac{k_{Probe}[Probe]_0}{k_{Probe}[Probe]_0 + \sum k_S[S]} \tag{S6}$$

with R_{Probe} being the rate of *Probe* reaction, with *RS* or other species, that can also be experimentally determined. By substituting (S6) in (S2) and solving for $R_{Product}^{-1}$ we obtain

$$R_{Product}^{-1} = \frac{\sum k_S[S]}{R_{RS} \cdot Y_{Product} \cdot k_{Probe}} \cdot [Probe]^{-1} + \frac{1}{R_{RS} \cdot Y_{Product}} \tag{S7}$$

this is a linear relation as function of $[Probe]^{-1}$. By linear interpolation of experimental data (Figure 2d), it is possible to obtain the slope and intercept of the line and their ratio, which is equal to

$$\frac{slope}{intercept} = \frac{\sum k_S[S]}{k_{Probe}} \tag{S8}$$

Thus, by knowing the value of k_{Probe}, we can obtain $\sum k_S[S]$, that can, in turn, be used to obtain $t_{1/2}$ according eq. (S3) and F_{RS} according to eq. (S6). Then we can calculate R_{RS} according to eq. (S2) and, last, $[RS]_{SS}$ according to eq. (S4).

The steady-state concentration of *RS* (according to eq. (S4)) is the ratio between the rate of formation of *RS* and the rates of all the contributions that lead to its consumption. The definition is slightly different from that by Anifowose et al.[8] They do not consider the term associated to the probe in the denominator, thus calculating the concentration in the condition of zero probe concentration. We prefer to keep that term and discuss the dependence of the results on it.

Optical emission spectroscopy experiments

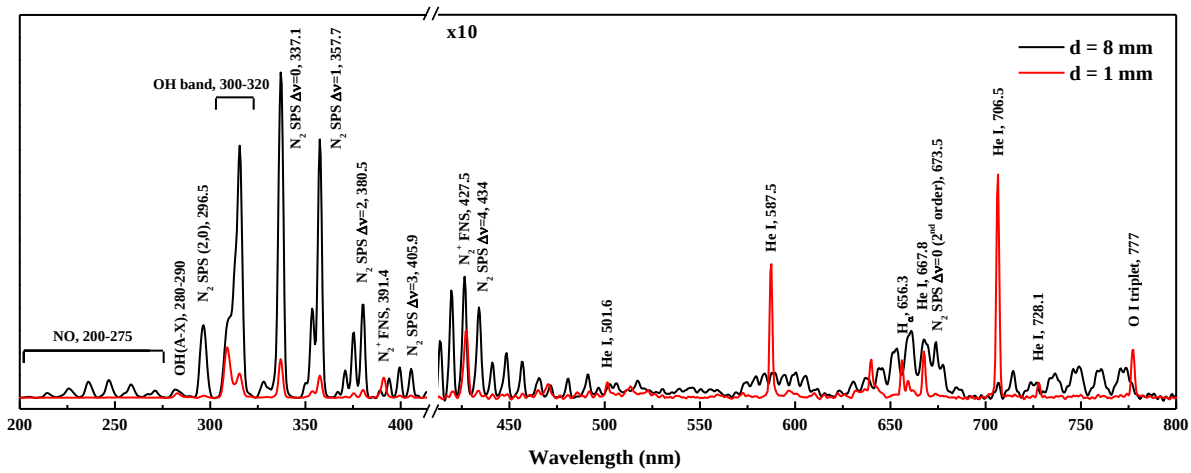

Figure S1. OES spectra for APPJ during treatment of ultrapure water 10 mm distance at 1 L/min He flow rate. Spectra are collected with the optical fibre at a vertical distance of 8 (black line) and 1 mm (red line) from the source; the spectra are multiplied by 10 between 400 and 800 nm to show the low-intensity lines (break shown in the x-axis).

Comparison between fluorescence and HPLC/UV-Vis

TPA is commonly used as probe to detect HO radicals in solution since it reacts to produce selectively hTPA that, unlike the reagents, is fluorescent.[10] By HPLC/UV-Vis analysis, we observed the formation of other minority products during plasma treatment of TPA solutions. Figure S2 reports a typical chromatogram and the areas of the main HPLC peaks as function of the plasma treatment time are reported.

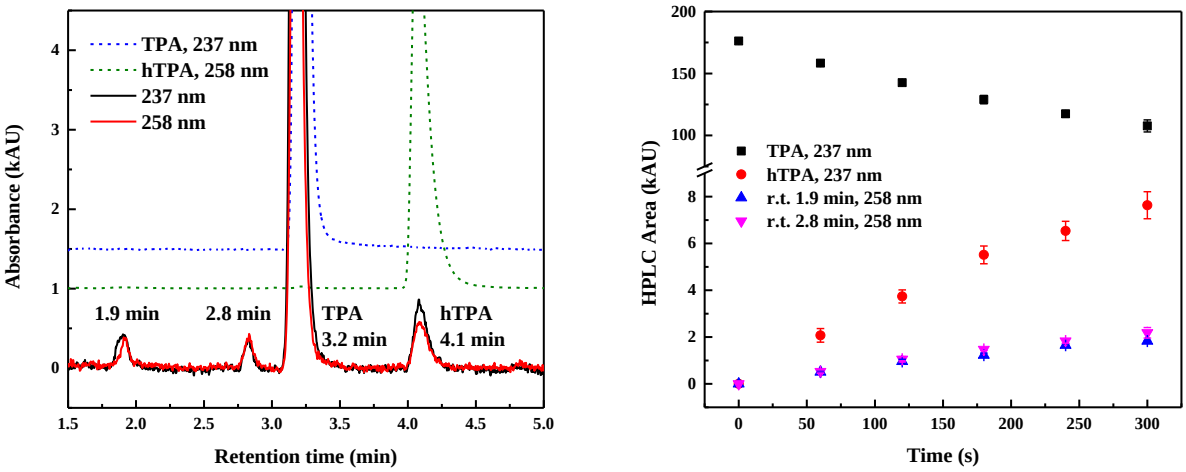

Figure S2. Left: Chromatograms at 237 and 258 nm of a 250 µM TPA solution in phosphate buffer (100 mM, pH 7) after 4 minutes of plasma treatment; chromatograms of untreated standard solutions of TPA and hTPA are reported as reference (dashed lines). Right: areas of the main peaks as function of plasma treatment time (right).

hTPA was the main product obtained by treating TPA, but at least other two species were produced at retention time of 1.9 min and 2.8 min, and their concentration increased linearly with treatment time. The formation of other products by reaction of TPA with HO radicals was already reported in the literature.[11] A comparison of the hTPA concentration obtained by fluorescence measurements (without chromatographic separation) and by HPLC/UV-Vis measurements is shown in Figure S3. Plasma treatment of TPA solutions produced other species besides hTPA, that have similar fluorescent properties. Without a chromatographic separation, the concentration of hTPA was overestimated by a factor of 1.5. Reproducibility was also better in the HPLC/UV analysis. For these reasons, all the results that are presented in this paper, related to hTPA quantification were obtained by HPLC/UV.

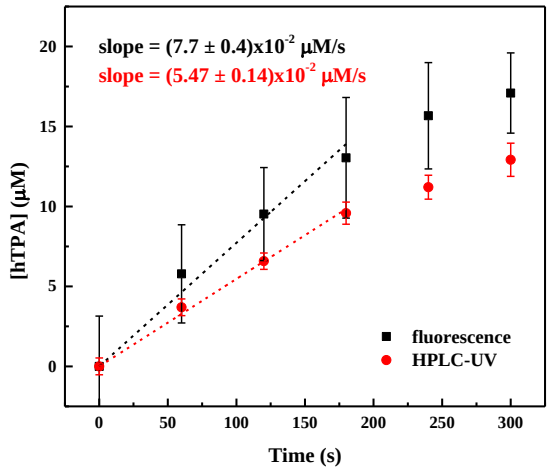

Figure S3. Concentration of hTPA produced by reaction of a 250 µM TPA solution in phosphate buffer (100 mM, pH 7) with plasma-generated HO radicals as function of plasma treatment time quantified by fluorescence spectroscopy ($\lambda_{ex/em}$ = 360/460 nm) and by HPLC/UV (λ = 237 nm).

Treatment of TPA solutions with different initial concentrations at pH 7

The decrease in TPA residual concentrations and the increasing concentrations of generated hTPA as function of the plasma treatment time for different initial concentrations in 100 mM PB at pH 7 are shown in Figure S4.

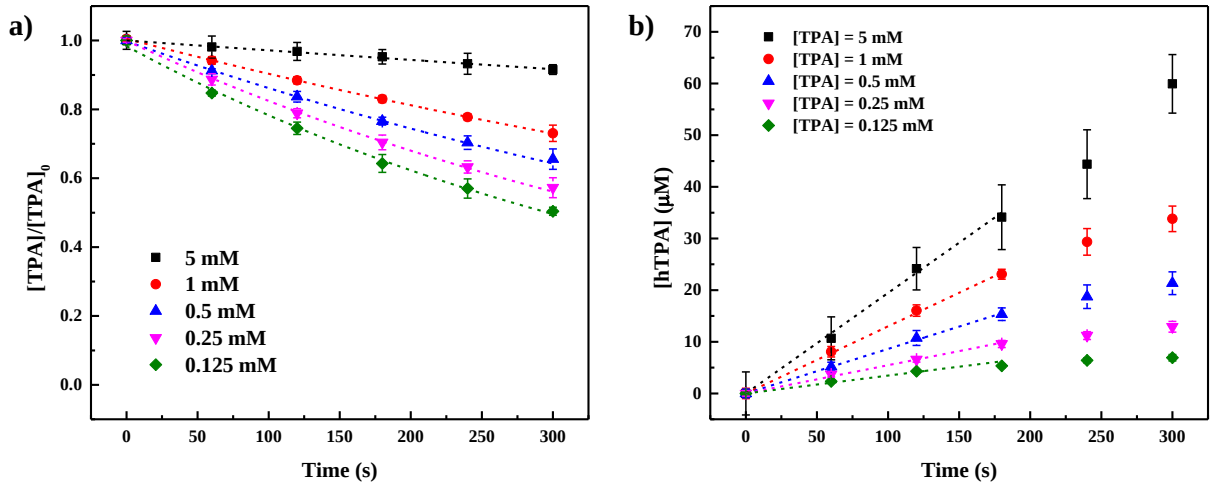

Figure S4. a) TPA residual concentration (normalized) as function of the treatment time for different initial nominal concentrations in PB 100 mM at pH 7; b) concentration of hTPA as function of the treatment time for different TPA initial nominal concentration in PB 100 mM at pH 7.

The rate of decrease of TPA concentration (R_{TPA}) and the rates of increase of hTPA concentration (R_{hTPA}) for all the initial TPA concentrations at pH 7 were obtained by fitting of the points in Figures S4a and S4b, using exponential and linear functions respectively and are reported in Figure S5. To calculate R_{hTPA}, only the experimental points corresponding to the shortest treatment times (max 180 s) were considered. Under this condition, the concentration of hTPA is 20 to 150 times lower than the concentration of TPA, thus the contribution of hTPA degradation due to CAP-generated RS can be considered negligible.

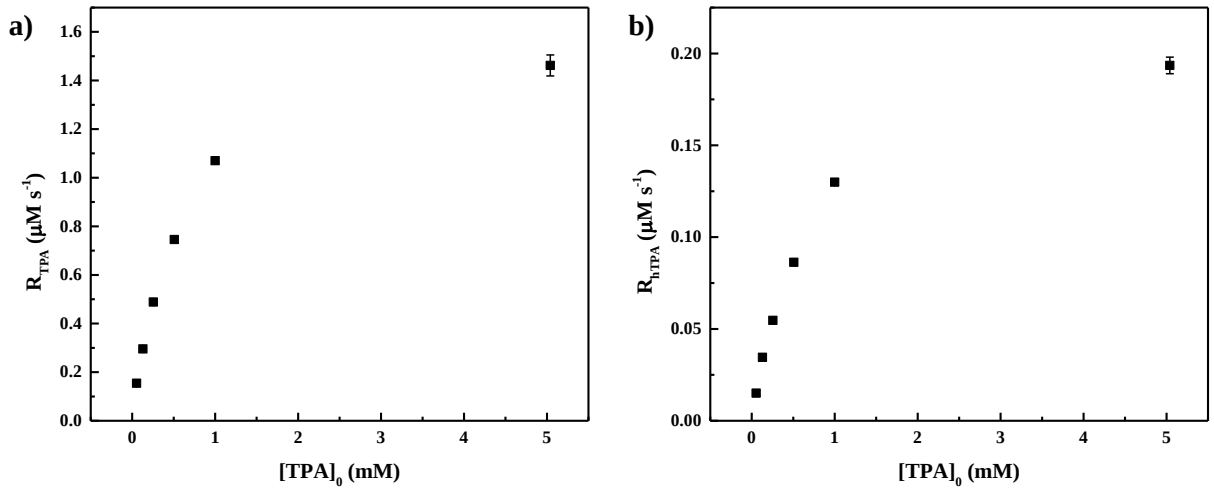

Figure S5. Rate of decrease of TPA concentration (a) and rate of increase of hTPA concentration (b) as a function of TPA real initial concentration at pH 7.

Calculation of the rate of formation of HO radicals, their lifetime and their steady state concentration at pH 3 and 7

Following the procedure reported above (eq. S7), we plotted the inverse of hTPA generation rates (R_{hTPA}^{-1}) versus the inverse of TPA starting concentration ($[TPA]_0^{-1}$) for the experiments performed at pH 3 and 7 (Fig. S6a), which led to very good linear correlations (Table S1).

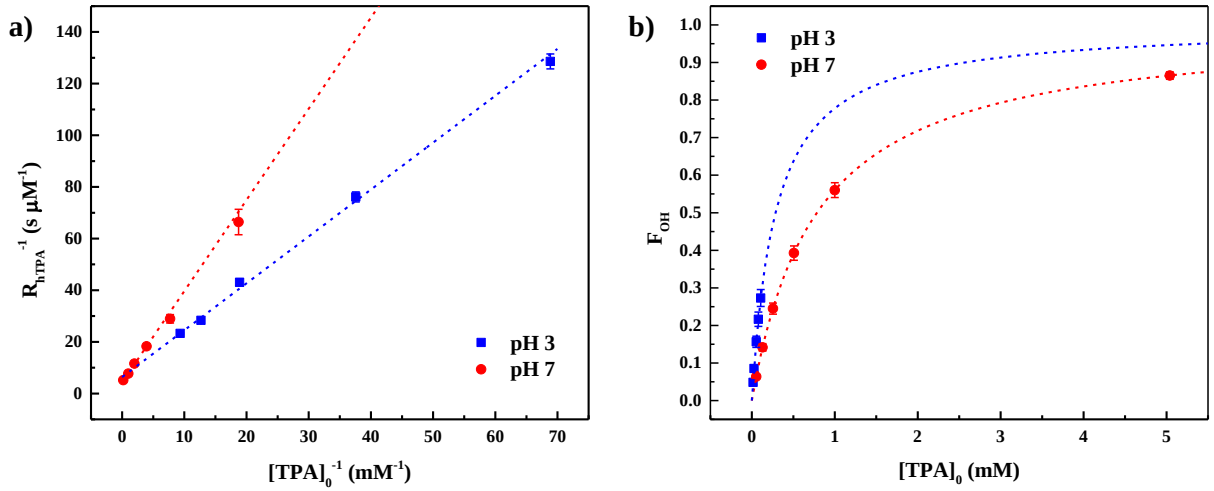

Figure S6. a) Reciprocal of hTPA formation rate (R_{hTPA}^{-1}) as a function of the reciprocal of $[TPA]_0$ at pH 3 (blue) and 7 (red). The dashed lines are the best linear interpolations of the experimental points. Parameters obtained from the interpolation are collected in Table S1. b) Fraction of plasma produced HO radicals that reacts with TPA as function of the probe starting concentration. The dashed lines are obtained using eq. S6.

Table S1. Parameters obtained from the linear interpolation of the data reported in Figure S6a.

	Slope (s)	**Intercept (s M^{-1})**	**R^2**
pH 3	$(1.82 \pm 0.05)\cdot10^3$	$(6.4 \pm 0.7)\cdot10^6$	0.996
pH 7	$(3.47 \pm 0.17)\cdot10^3$	$(4.42 \pm 0.24)\cdot10^6$	0.992

From the interpolation of the points in Figure S6a we calculated the slope/intercept ratios that are equal to $\sum k_S[S]/k_{TPA}$. We obtained $(2.9 \pm 0.3)\cdot10^{-4}$ M at pH 3 and $(7.9 \pm 0.6)\cdot10^{-4}$ M at pH 7. From these values, using the value for k_{TPA} reported in the literature $(4.4 \pm 0.1)\cdot10^9$ M^{-1} s^{-1},[12] we obtained the rate of all the processes - other than the reaction with TPA- that lead to HO· consumption: $(1.26 \pm 0.14)\cdot10^6$ s^{-1} at pH 3 and $(3.45 \pm 0.26)\cdot10^6$ s^{-1} at pH 7.

This allowed to calculate the half-life time ($t_{1/2}$) of HO radicals in solution according to eq. S3 (reported in Table 1 in the manuscript) and the fraction of HO· that reacts with TPA (eq. S6). The latter is reported in Figure S6b as function of TPA initial concentration, for pH 3 and 7. Last, we used the values of F_{OH} to calculate R_{HO} according to eq. (S2) and $[HO]_{SS}$ according to eq. (S4). Both values are reported in Table 1 in the manuscript.

Acid-base equilibria of the main species produced by plasma in liquids

In Table S2 are collected the pKa corresponding to the acid-base equilibria of the main species produced by plasma treatment of a water solution in presence of ambient air.

Table S2. Acid-base equilibria of main plasma-produced species

Acid-base equilibria		pK_a	Ref
S9	$HO^{\cdot} + H_2O \rightleftarrows O^{-\cdot} + H_3O^+$	11.8	13
S10	$HO_2^{\cdot} + H_2O \rightleftarrows O_2^{-\cdot} + H_3O^+$	4.8	14
S11	$HO_3^{\cdot} + H_2O \rightleftarrows O_3^{-\cdot} + H_3O^+$	-2.1	13
S12	$H_2O_2 + H_2O \rightleftarrows HO_2^- + H_3O^+$	11.6	14
S13	$HNO_2 + H_2O \rightleftarrows NO_2^- + H_3O^+$	3.4	15
S14	$HNO_3 + H_2O \rightleftarrows NO_3^- + H_3O^+$	-1.4	15
S15	$HOONO + H_2O \rightleftarrows OONO^- + H_3O^+$	6.5	16

Reactions of plasma-generated RS in solution contributing to HO· generation

HO radicals can be generated through many different pathways in the gas phase, in the liquid phase by reaction of gas-phase species with water or by decomposition of other reactive species in solution.[17] Here we focus only on the last processes because they can be dependent on the pH of the solution. These are summarized in Table S1.

Table S3. Reactions of production of hydroxyl radicals in plasma-treated water solution.

HO· production in solution		Ref
S16a	$O_3 + HO_2^{\cdot} \rightarrow O_2 + HO_3^{\cdot}$	17
S16b	$HO_3^{\cdot} \rightarrow HO^{\cdot} + O_2$	17
S17a	$O_3 + O_2^{-\cdot} \rightarrow O_2 + O_3^{-\cdot}$	9
S17b	$O_3^{-\cdot} \rightarrow O^{-\cdot} + O_2$	9
S17c	$O^{-\cdot} + H_2O \rightarrow HO^{\cdot} + HO^-$	9
S18a	$H_2O_2 + NO_2^- + H_3O^+ \rightarrow HOONO + 2H_2O$	17
S18b	$HOONO \xrightarrow{pH<6} HO^{\cdot} + NO_2^{\cdot}$	17
S19	$O_3 + H_2O_2 \xrightarrow{pH>5} HO^{\cdot} + HO_2^{\cdot} + O_2$	17
S20	$O_3 + HO_2^- \rightarrow O_2 + O_2^{-\cdot} + HO^{\cdot}$	18
S21	$H_2O_2 + H^{\cdot} \rightarrow H_2O + HO^{\cdot}$	18
S22	$H_2O_2 + e^-_{(aq)} \rightarrow HO^{\cdot} + HO^-$	18
S23	$H_2O_2 + O_2^{-\cdot} \rightarrow HO^{\cdot} + HO^- + O_2$	9

Reaction of ozone with superoxide produces HO radicals both at acidic and neutral pH (eq.s S16 and S17). Reaction of hydrogen peroxide with nitrite ions is favoured at acidic pH (eq. S18) while the one with ozone at neutral-basic pH (eq.s S19 and S20). Haber-Weiss reaction between hydrogen peroxide and superoxide (eq. S23) occurs in the presence of transition metals at neutral-basic pH. Reactions of hydrogen peroxide with hydrogen atoms or solvated electrons are expected to be pH-independent (eq.s S21 and S22).

References

(1) Zaplotnik, R.; Bišćan, M.; Kregar, Z.; Cvelbar, U.; Mozetič, M.; Milošević, S. Influence of a Sample Surface on Single Electrode Atmospheric Plasma Jet Parameters. *Spectrochim. Acta Part B At. Spectrosc.* **2015**, *103–104*, 124–130. https://doi.org/10.1016/j.sab.2014.12.004.

(2) Canal, C.; Modic, M.; Cvelbar, U.; Ginebra, M.-P. Regulating the Antibiotic Drug Release from β-Tricalcium Phosphate Ceramics by Atmospheric Plasma Surface Engineering. *Biomater. Sci.* **2016**, *4* (10), 1454–1461. https://doi.org/10.1039/C6BM00411C.

(3) Tornin, J.; Mateu-Sanz, M.; Rodríguez, A.; Labay, C.; Rodríguez, R.; Canal, C. Pyruvate Plays a Main Role in the Antitumoral Selectivity of Cold Atmospheric Plasma in Osteosarcoma. *Sci. Rep.* **2019**, *9* (1), 10681. https://doi.org/10.1038/s41598-019-47128-1.

(4) Labay, C.; Hamouda, I.; Tampieri, F.; Ginebra, M.-P.; Canal, C. Production of Reactive Species in Alginate Hydrogels for Cold Atmospheric Plasma-Based Therapiesle. *Sci. Rep.* **2019**, *9*, 16160. https://doi.org/10.1038/s41598-019-52673-w.

(5) Liao, C.-H.; Kang, S.-F.; Wu, F.-A. Hydroxyl Radical Scavenging Role of Chloride and Bicarbonate Ions in the H2O2/UV Process. *Chemosphere* **2001**, *44* (5), 1193–1200. https://doi.org/10.1016/S0045-6535(00)00278-2.

(6) Brown, H. C.; McDaniel, D. H.; Häfliger, O. Dissociation Constants. In *Determination of Organic Structures by Physical Methods - Volume 1*; Baude, E. A., Nachod, F. C., Eds.; Elsevier: New York, NY, 1955; pp 567–662. https://doi.org/10.1016/C2013-0-12413-0.

(7) Yalkowsky, S. H.; He, Y.; Jain, P. *Handbook of Aqueous Solubility Data*, 2nd ed.; CRC Press: Boca Raton, FL, 2010.

(8) Anifowose, A. J.; Takeda, K.; Sakugawa, H. Novel Fluorometric Method for the Determination of Production Rate and Steady-State Concentration of Photochemically Generated Superoxide Radical in Seawater Using 3′,6′-(Diphenylphosphinyl)fluorescein. *Anal. Chem.* **2015**, *87* (24), 11998–12005. https://doi.org/10.1021/acs.analchem.5b00917.

(9) Cabrellon, G.; Tampieri, F.; Rossa, A.; Barbon, A.; Marotta, E.; Paradisi, C. Application of Fluorescence Based Probes for the Determination of Superoxide in Water Treated with Air Non-Thermal Plasma. *ACS Sensors* **2020**, acssensors.0c01042. https://doi.org/10.1021/acssensors.0c01042.

(10) Saran, M.; Summer, K. H. Assaying for Hydroxyl Radicals: Hydroxylated Terephthalate Is a Superior Fluorescence Marker than Hydroxylated Benzoate. *Free Radic. Res.* **1999**, *31* (5), 429–436. https://doi.org/10.1080/10715769900300991.

(11) Fang, X.; Mark, G.; von Sonntag, C. OH Radical Formation by Ultrasound in Aqueous Solutions Part I: The Chemistry Underlying the Terephthalate Dosimeter. *Ultrason. Sonochem.*

1996, *3* (1), 57–63. https://doi.org/10.1016/1350-4177(95)00032-1.

(12) Page, S. E.; Arnold, W. A.; McNeill, K. Terephthalate as a Probe for Photochemically Generated Hydroxyl Radical. *J. Environ. Monit.* **2010**, *12* (9), 1658. https://doi.org/10.1039/c0em00160k.

(13) Naumov, S.; von Sonntag, C. The Reaction of •OH with O2, the Decay of O 3•− and the pKa of HO 3• - Interrelated Questions in Aqueous Free-Radical Chemistry. *J. Phys. Org. Chem.* **2011**, *24* (7), 600–602. https://doi.org/10.1002/poc.1812.

(14) Tampieri, F.; Cabrellon, G.; Rossa, A.; Barbon, A.; Marotta, E.; Paradisi, C. Comment on "Water-Soluble Fluorescent Probe with Dual Mitochondria/Lysosome Targetability for Selective Superoxide Detection in Live Cells and in Zebrafish Embryos." *ACS Sensors* **2019**, *4* (11), 3080–3083. https://doi.org/10.1021/acssensors.9b01358.

(15) Ripin, D. H.; Evans, D. A. Evans pKa Table. *The Evans Group*. 2005.

(16) Hughes, M. N. Chemistry of Nitric Oxide and Related Species. In *Globins and Other Nitric Oxide-Reactive Proteins, Part A*; Poole, R. K., Ed.; Elsevier, 2008; pp 3–19. https://doi.org/10.1016/S0076-6879(08)36001-7.

(17) Nani, L.; Tampieri, F.; Ceriani, E.; Marotta, E.; Paradisi, C. ROS Production and Removal of the Herbicide Metolachlor by Air Non-Thermal Plasma Produced by DBD, DC- and DC+ Discharges Implemented within the Same Reactor. *J. Phys. D. Appl. Phys.* **2018**, *51* (27), 274002. https://doi.org/10.1088/1361-6463/aab8b9.

(18) Locke, B. R.; Shih, K.-Y. Review of the Methods to Form Hydrogen Peroxide in Electrical Discharge Plasma with Liquid Water. *Plasma Sources Sci. Technol.* **2011**, *20* (3), 34006. https://doi.org/10.1088/0963-0252/20/3/034006.